Volume 1 | Number 1 | Jan 2013 | Pages 1–100

Nanoscale

www.rsc.org/nanoscale

ROYAL SOCIETY
OF CHEMISTRY

ROYAL SOCIETY
OF CHEMISTRY

www.rsc.org/nanoscale

Journal Name

Nanoscale

ARTICLE TYPE

Incorporation of Cl in sequentially deposited lead halide perovskite films for highly efficient mesoporous solar cells.

Sabba Dharani[a,b], Herlina Arianita Dewi[b], Rajiv Ramanujam Prabhakar[b], Tom Baikie[b], Chen Shi[c], Du Yonghua[d], Nripan Mathews[a,b,e], Pablo P. Boix[b]*, Subodh G. Mhaisalkar[a,b]*

Organic-inorganic lead halide perovskites have been widely used as an absorber on mesoporous TiO_2 films as well as a thin film in planar heterojunction solar cells, yielding very high photovoltaic conversion efficiencies. Both the addition of chloride and sequential deposition methods have been successfully
10 employed to enhance the photovoltaic performance. Here, both approaches are combined in a sequential method by spincoating $PbCl_2 + PbI_2$ on a mesoporous TiO_2 film followed by the perovskite transformation. The role of Cl determining the optical, electrical, structural and morphological properties is correlated with the photovoltaic performance. The highest photovoltaic efficiency of 14.15 % with the V_{oc}, FF and J_{sc} being 1.09 V, 0.65 and 19.91 mA/cm^2 respectively, was achieved with a 10 mol % of
15 $PbCl_2$ addition due to an increase of the film conductivity induced by a better perovskite morphology. This is linked to an improvement of the hysteresis and reproducibility of the solar cells.

Introduction

Organic-inorganic halide perovskite ($CH_3NH_3PbI_3$, $CH_3NH_3PbI_{3-}$
20 $_xCl_x$) solar cells have gained immense technological and scientific interest as they are highly efficient ($\eta > 17$ %)[1] and have diffusion lengths in the range of 100-1000 nm.[2-4] The ease of depositing the perovskite layer from solution has increased the research in this area exponentially.[5, 6] In particular, two different
25 solution deposition techniques are widely utilised: the single step deposition where all the precursors are dissolved and deposited together[7] and the sequential deposition, where the precursors are deposited in two subsequent steps[5]. These processes will determine the distribution of the perovskite within the
30 mesoporous structure, with the sequential deposition technique achieving better coverage with more homogenous films[5]. In this regard, studies on the role of perovskite pore filling in the TiO_2 scaffold[8,9] have shown that having an overlayer of the perovskite on the mesoporous TiO_2 prevents the recombination between the
35 photo-injected electrons and the hole transporting material, resulting in enhancement of the photovoltage[8].

Another reported approach to improve charge transport has exploited the introduction of chloride in the fabrication of the perovskite[10]. Although several works have shown a variation in
40 the device properties, the ultimate effect of the Cl-addition is still not clear[10-13]. In addition, most of those Cl-effect studies have focused extensively on single step perovskite deposition and not much research on sequentially depositing mixed halide solar cells for investigating the role of the halide has been reported so far.

45 Herein, we show a sequential method to obtain mixed halide perovskite based solar cells where chloride was introduced into the system as $PbCl_2$ in mol %. This deposition technique yields homogeneous films with good surface coverage as well as better
50 reproducibility of cell performance. We systematically investigate the effect of chloride in the photovoltaic performance by decoupling the optical, electrical and morphological effects. When a controlled amount of Cl was employed in the perovskite formation process, the photovoltaic performance of the cell
55 improved to more than 14 % efficiency. This was justified with a decrease in sheet resistance caused by an increase in the film conductivity, as detected by 4-probe resistivity measurements. Although the inclusion of Cl did not affect the band-gap or lattice parameters of the perovskite material, it had a strong influence on
60 the morphological evolution of the crystals which altered the resistivity/conductivity of the film. The effect on the final device mechanisms was mainly observed in a decrease of the low frequency capacitance, which we tentatively assign to an improvement of the hysteresis and reproducibility when
65 cyclic voltammetry was measured.

Results and discussion

For the formation of $CH_3NH_3PbI_{3-x}Cl_x$, we followed procedures
70 in line with that reported for the sequential deposition of

$CH_3NH_3PbI_3$ by Burschka et.al[5]. However, due to the poor solubility of $PbCl_2$ in dimethylformamide (DMF), only low concentrations of $PbCl_2$ could be employed (~ 0.1 M) resulting in a poor loading of the perovskite (as shown in Fig. S1). The solubility limitation could be circumvented by preparing mixed solutions of $PbCl_2$ along with 1 M of PbI_2[12]. For XRD characterization of 1 M $PbCl_2$, dimethyl sulfoxide (DMSO) solvent was used. So when pure $PbCl_2$ was spin coated and exposed to CH_3NH_3I in IPA, a brown colored film was formed. XRD measurements indicated strong (110) and (220) peaks which were indexed to $CH_3NH_3PbI_3$ along with a large amorphous contribution (Fig. 1a).
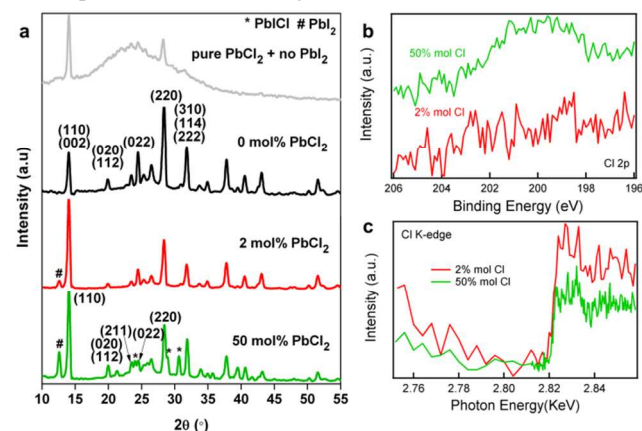

Fig.1 (a) XRD patterns of perovskite samples prepared by using only $PbCl_2/PbI_2$ and mixture of $PbCl_2$ and PbI_2 in MAI. (b) Cl 2p spectra and (c) XAS spectra at Cl *K*-edge for the perovskite samples with 2 and 50 mol % of $PbCl_2$ addition.

Fig. 1a also shows the powder X-ray diffraction patterns for perovskites films on mesoporous TiO_2 prepared with 0, 2 and 50 mol % of $PbCl_2$. For the pattern obtained with no addition of $PbCl_2$ (0 mol % sample) the reflections observed are entirely consistent with the previous reports for the iodide perovskite[14], with additional weak reflections from the FTO/TiO_2 substrate. For this sample no additional PbI_2 peak was observed, which is interpreted as a complete $CH_3NH_3PbI_3$ formation. For a 2 mol % addition of $PbCl_2$, the reflections measured after the perovskite conversion are fully consistent with the pure $CH_3NH_3PbI_3$. Although no noticeable peak shift indicating a change in lattice parameters was observed, there is an enhanced intensity of the (110) reflection which indicates an increase of the preferential orientation of the perovskite crystals, together with a small contribution from the (001) reflection of the 2H-polymorph of PbI_2. Similarly, samples with 50 mol % addition of $PbCl_2$ show no variation in reflection position for the iodide perovskite peaks. In this case, the noticeable enhancement of the (110) comes along with an apparent disappearance of the (002) reflection. Such a preferred orientation effect is probably related to the Cl addition favouring the growth of the perovskite crystallites along a particular crystallographic direction[10]. In addition to the perovskite reflections, the 50 mol % of $PbCl_2$ has an enhanced intensity for the (001) reflection of PbI_2 with an additional presence of PbICl. For a successful substitution of I by Cl in the perovskite structure a reduction in lattice parameters would be expected, as observed previously in the $MAPbI_{3-x}Br_x$[15] and $MAPbI_{3-x}Cl_x$[10]. However in this work, no change in the lattice parameters was observed (Table. S1) which is in agreement with the observation made by Docampo et al[16].

To further unravel the presence of Cl in mixed halide samples XPS and XAS measurements were performed. XPS result show a Cl 2p peak is present in the sample with 50 mol %, while Cl 2p peak in 2 mol % sample is below the detection limits of XPS (Fig. 1b). The concentration of Cl in 50 mol % sample is around 0.7 %, which is in good agreement with previous reports[10]. Because XPS is only sensitive to surfaces, XAS measurements in fluorescence mode were also performed to check the presence of Cl in bulk. In Fig. 1c, a rise at Cl *K*-edge is observed in both samples, which confirms the presence of Cl. It is worth to remark that the detection of Cl with these techniques does not necessarily imply a doping of perovskite with the incorporation of Cl into the structure.

ARTICLE TYPE

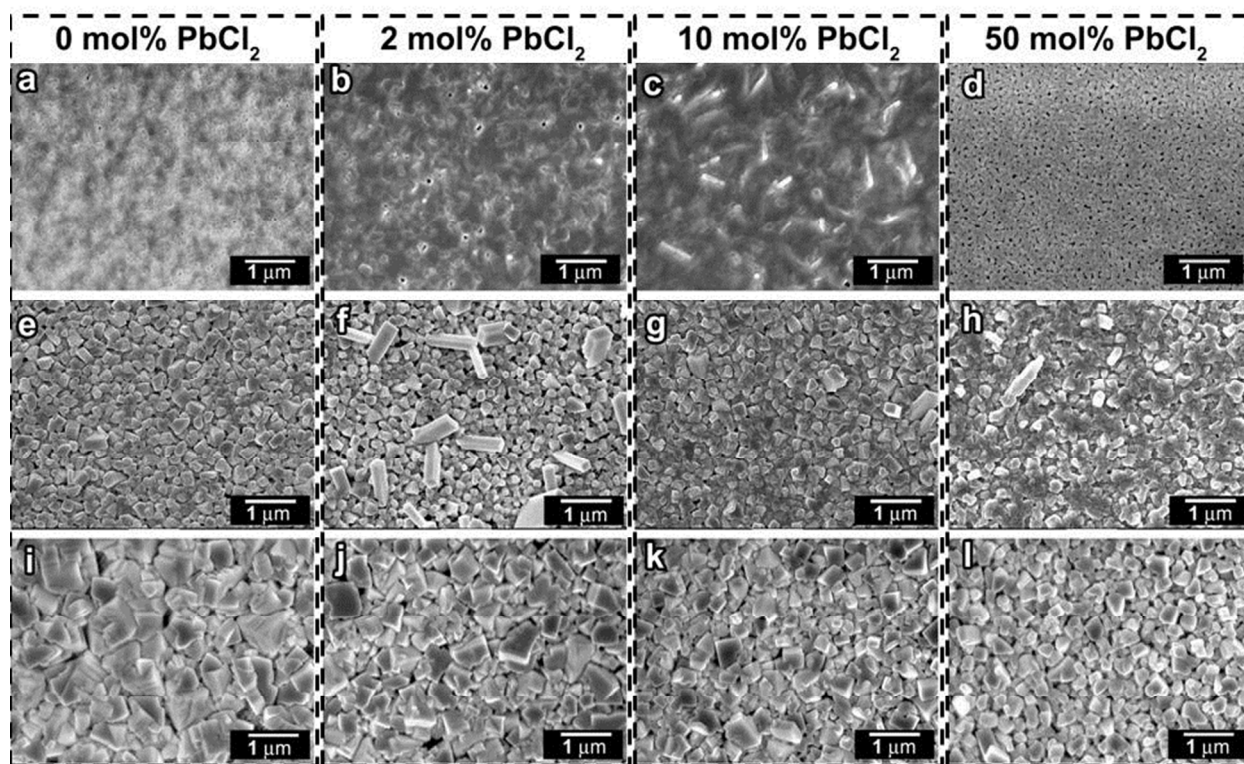**Fig.2** Top-view FESEM images illustrating surface coverage and morphological evolution with addition of Cl. (a,b,c & d) represent PbI_2+ x mol % $PbCl_2$ (x being 0, 2, 10 and 50 respectively) samples, whereas (e,f,g & h) represent their corresponding morphologies after perovskite conversion when annealed at 70 °C and at 100 °C (i,j,k & l).

From the FESEM images (Fig. 2 (a,b,c,d)), the evolution in morphology as a function of $PbCl_2$ concentration was clear after the first step of sequential deposition - spin coating of 1 M of PbI_2 + x mol % $PbCl_2$ (x = 0, 2, 10, 50) dissolved in DMF solution. As the Cl concentration was increased to 10 mol %, the lead halide film became more and more compact, with rod like nanostructures projecting especially for 10 mol % $PbCl_2$ sample (Fig. 2c). In contrast, in the sample with 50 mol % of $PbCl_2$, the lead halide film exhibited a more porous nature (Fig. 2d). When these films were reacted with a CH_3NH_3I solution in IPA, it was observed that perovskite coverage on the mesoporous film improved with closer packing of the perovskite crystals upon increasing $PbCl_2$ concentration (Fig. 2 (e,f,g,h)). In addition to the compact packing of the perovskite crystals, the increase of $PbCl_2$

concentration also generated pillar-like projections which increased the film roughness dramatically. Furthermore, upon annealing these films at 100 °C, the average perovskite crystal size increased for $CH_3NH_3PbI_3$ (no Cl addition) but the film coverage was not improved, as it is shown in Fig. 2i. The increase of the average crystal size after the 100 °C annealing is also observed in the samples with Cl, ($PbCl_2$ = 2, 10 and 50 mol %). However, the crystal size decreased with increasing $PbCl_2$ concentration i.e crystal size of (l) < crystal size (k) < crystal size (j) < crystal size (i). Interestingly, the film coverage improved and the pillar like projections were no longer observed (Fig. 2 (j,k,l)). These top view FESEM images confirmed that the addition of $PbCl_2$ in the initial film results in a significant change in the morphology with respect to the pure $CH_3NH_3PbI_3$
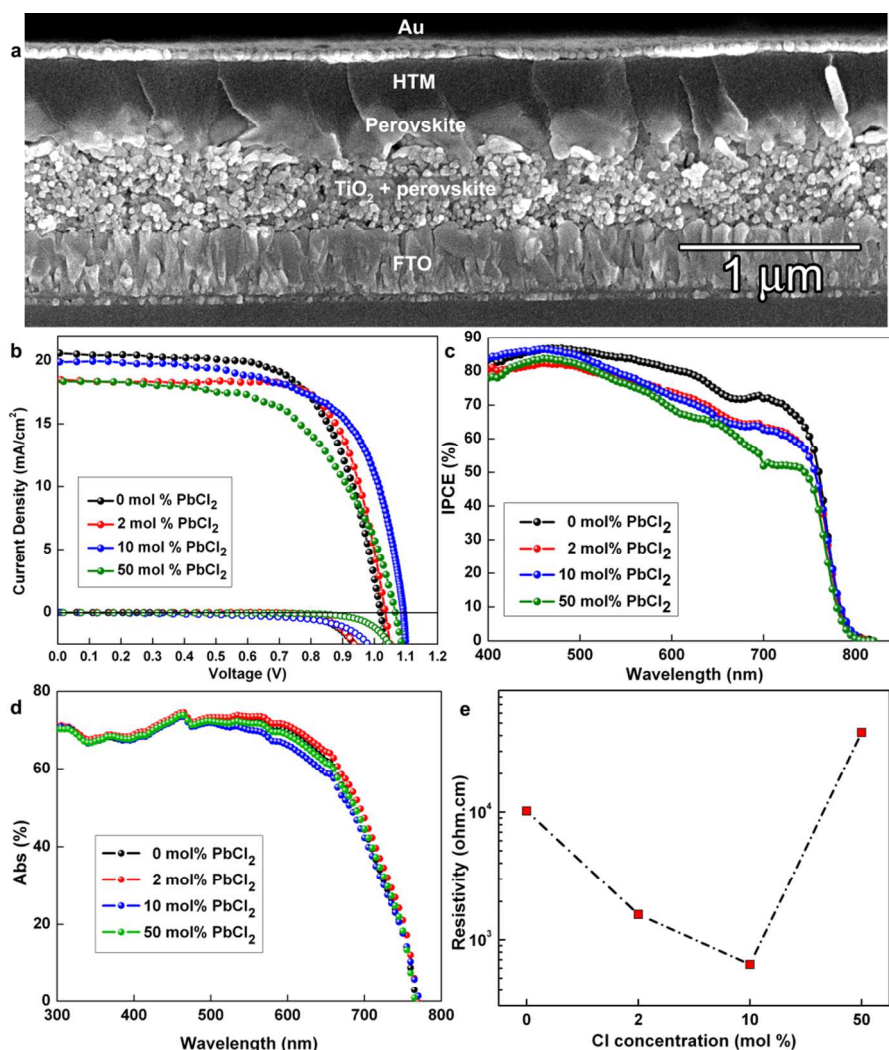
Nanoscale Accepted Manuscript

ARTICLE TYPE

Fig3 (a) Cross-sectional FESEM image of a full device, (b) J-V and (c) IPCE of the champion cells, (d) optical absorption spectra of perovskites with different initial $PbCl_2$ concentrations on mesoporous TiO_2 and (e) four probe resistivity of representative perovskite films.

As a result, the effect of addition of $PbCl_2$ was reflected in the performance of the solar cells in terms of J-V characteristics. Fig.
5 3a shows the cross-sectional FESEM image of a representative full solar cell from which it is evident that the perovskite ($CH_3NH_3PbI_3$) layer was ~250 nm while the spiro-OMeTAD overlayer was ~260 nm. Similarly, the perovskite overlayer thickness for the 20 mol % sample was measured to be 280-573
10 nm (Fig. S3a). For the 50 mol % of $PbCl_2$ sample (Fig. S3b), the perovskite overlayer thickness increased to 411-790 nm, however the presence of the hole transporting material (HTM) overlayer enabled a benign interface thereby facilitating average performance of the cell. The J-V characteristics as well as the
15 integrated current densities of the champion cells are tabulated in Table 1 and represented in Fig. 3a.

Table. 1 J-V characteristics of best cells for different concentrations of Cl.

$PbCl_2$ (mol %)	J_{sc} (mA/cm^2)	V_{oc} (V)	FF	η (%)	Integrated J_{sc} (mA/cm^2)
0	20.59	1.02	0.62	13.81	19.7
2	18.50	1.03	0.73	13.91	18.19
10	19.91	1.09	0.65	14.15	18.45
50	18.38	1.07	0.59	11.57	17.27

20 The best efficiency of 14.15 % was observed for 10 mol% of $PbCl_2$ with the V_{oc}, FF and J_{sc} being 1.09 V, 0.65 and 19.91 mA/cm^2 respectively (Table. 1 and Fig. 3a). Also from the IPCE

spectrum (Fig. 3b), the short circuit current density (J_{sc}) was integrated to be 18.45 mA/cm^2, which complies well with the J_{sc} measured from the J-V measurements. Interestingly from Fig. 3(b and c) no change in the onset of IPCE and absorption spectra
5 were observed for samples with and without Cl addition, clearly implying that the addition of Cl does not cause any band gap modification. The cell performance improved only marginally when PbCl$_2$ was added for concentrations ≤10 mol % and it decreased for higher concentrations. These trends are confirmed
10 by the average results (> 8 samples) represented in Table 2. The depreciation in cell performance for higher concentrations is reflected by the declining FF and J_{sc}. In order to discern the origin for this drop in performance, 4-probe resistivity measurements were measured on the perovskite films. From Fig. 3d, it is evident
15 that for 2 and 10 mol % of PbCl$_2$ addition, the resistivity of the films decreased by an order of magnitude in comparison to Cl-free lead perovskite. Further increase of the Cl concentration to 50 mol % resulted in increased resistivity, overcoming that of Cl free perovskite, which accounts for the lowering of FF.

20 **Table. 2** Effect of addition of Cl on average photovoltaic parameters of perovskite based solar cells with error bars on at least 8 samples.

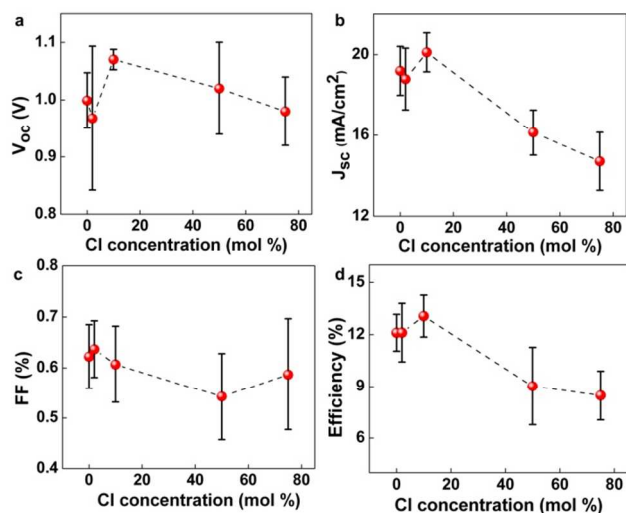| PbCl$_2$ (mol %)	J_{sc} (mA/cm^2)	V_{oc} (V)	FF	η (%)
0	19.19±1.21	0.99±0.05	0.62±0.062	12.1±1.1
2	18.79±1.52	0.97±0.13	0.64±0.055	12.10±0.7
10	20.11±0.96	1.07±0.18	0.61±0.075	13.1±1.2
50	16.14±1.12	1.02±0.08	0.54±0.085	9.0±2.2
75	14.71±1.43	0.98±0.06	0.59±0.109	8.5±1.4

Fig.4 Statistical distribution of J-V parameters with varying Cl concentration (mol %).

25 The average performances of all the measured solar cells presented in Fig. 4 and Table 2, show the trend for highest J_{sc} (20.11 ± 0.96 mA/cm^2) and V_{oc} (1.07 ± 0.18 V) observed for the 10 mol % of PbCl$_2$ sample, along with a lower dispersion of parameters which accounts for a slightly improvement of the
30 reproducibility. This is explained by the low resistivity and better coverage of the perovskite film which might enable better charge transport. In order to elucidate further electrical effects upon the addition of Cl, impedance spectroscopy measurements was

performed for 0% and 10% samples, representative of the general
35 trend displayed in Table 2 (Cl free sample showed 18.52 mA/cm^2 of J_{sc}, 1.05 V of V_{oc}, 0.58 FF and 11.27 % of efficiency under 1 sun illumination and 10 mol % of PbCl$_2$ sample exhibited 1.07 V of V_{oc}, 19.24 mA/cm^2 of J_{sc}, 0.61 of FF and 12.55 % of efficiency) under illumination. The results were fitted with an
40 equivalent circuit previously reported[17]. The high frequency part of the spectra, which is ascribed to the hole transport phenomena[18-20], show as expected, identical behaviour regardless of the absorber composition (Fig. 5a,b). Similarly, the recombination resistance (R_{rec}), extracted from the lower
45 frequency part of the spectra, reveals analogous values for the tri-iodine sample and the mixed halide perovskite sample (10 mol % of PbCl$_2$) (Fig. 5a), in contrast with previous reports based on single step deposition techniques where the recombination was significantly reduced upon the Cl addition[13, 21]. As a result, the
50 differences in the performance cannot be attributed to a modification of the measured recombination process. **Similarly, the small improvement of the V_{oc} has to be ascribed to the increased charge generation, which is reflected in a higher J_{sc} as well.**
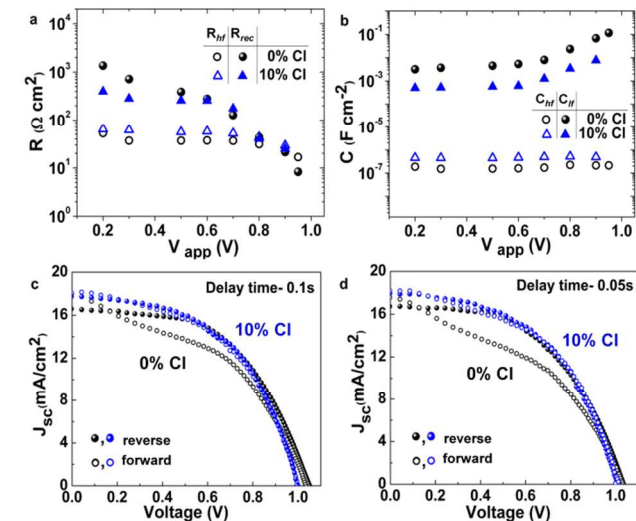

55

Fig.5 (a) Resistance vs. applied voltage where the filled symbols denote R_{rec} while R_{HF} is represented by the empty symbols, (b) Capacitance vs. applied voltage plots with the filled symbols marking C_{LF} and the empty ones that of C_{HF} and (c) and (d) illustrate the hysteresis for the chlorine
60 free and 10 mol % of PbCl$_2$ perovskite cells at different scan rates.

However, the fitting of both samples show remarkably different capacitance values obtained from the low frequency region of the spectra (Fig. 5b). These values appear to be too high to be related to the TiO$_2$ chemical capacitance[22, 23]. We tentatively attribute the
65 lower value of the 10 mol % PbCl$_2$ sample to its higher conductivity. Interestingly, this comes along with a significant lower hysteresis in the J-V curves (Fig. 5(c,d)). Hysteresis for different scan rates has been quantified in both the samples using the hysteric index (HI)[24] and tabulated in Table S3. The observed
70 hysteresis is lower for the samples with 10 mol % PbCl$_2$ addition and the trend of declining hysteresis with faster scan rates for both the samples is in concurrence with the earlier reports[25]. A full study of this capacitance, which is out of the scope of this work, will be required to further understand the implications.

Therefore, the slight efficiency boost observed when small concentrations of $PbCl_2$ were employed in the sequential deposition is mainly attributed to a morphological effect, which generates an increase of the conductivity of the film. This is in good agreement with previous reports[10, 16] showing that the addition of a limited amount of Cl in single step or sequential deposition techniques improved charge transport. However, further addition of Cl degrades the cell performance (η < 10 %, Fig. 4d) mainly by the degrading FF and J_{sc}, which is ascribed to a poor charge collection associated with the increase of the resistivity of the perovskite film.

Conclusions

Detailed investigation on the morphological, optical and electrical properties of a mixed halide perovskite deposited by employing sequential deposition technique was carried out. Cl concentration was varied and a systematic approach was employed to understand its implications on the various parameters of an efficient solar cell. The addition of low amounts of Cl improves the solar cell performance, mainly due to an increase of the perovskite conductivity. The system demonstrated a threshold limit of 10 mol % of $PbCl_2$ addition beyond which the advantage of Cl addition was negated by the poor FF and lower J_{sc} which could be attributed to lower charge collection owing to the high film resistivity. Addition of Cl had no effect on the absorption of the films but it altered the morphology of the perovskite crystals, thereby affecting the I-V characteristics of solar cell.

Experimental

Device fabrication: Fluorine doped tin oxide glass substrates (Tec15, <14 ohm/square, 2.2 mm thick, Pilkington) were patterned by laser etching and were subsequently cleaned by ultrasonication in decon soap solution followed by rinsing with deionized water and ethanol. They were further ultrasonicated in ethanol and were dried with clean dry air. A compact TiO_2 blocking layer was deposited by treating the cleaned substrates with 200 mM $TiCl_4$ solution at 70 ^oC for 1 h[26] followed by sintering at 500 ^oC in air for 1-3 h. Then a mesoporous TiO_2 film was spincoated at 4000 rpm for 30 s and was dried at 120.5 ^oC for 10 min which was followed by sintering at 500 ^oC for 15 min. For mesoporous TiO_2 film (300-400 nm), Dyesol 30 NRD was used in absolute ethanol in the ratio 2:7 by volume. They were then subjected to 20 mM $TiCl_4$ treatment at 70 ^oC for 30 mins followed by sintering at 500 ^oC in air for 15 min. For the synthesis of $CH_3NH_3PbI_{3-x}Cl_x$ perovskite, PbI_2 (1 M), $PbCl_2$ (1 M) and mixture of PbI_2 (1 M kept constant for all the samples) and $PbCl_2$ (mol % = 2, 10, 50, 75 which corresponds to 0.02 M, 0.1 M, 0.5 M and 0.75 M respectively) were dissolved in DMF at 70 ^oC respectively. Since 1M of $PbCl_2$ has solubility issues with DMF, DMSO solution was used. These solutions were spincoated on the mesoporous TiO_2 films at 6000 rpm for 5 s and were dried at 70 ^oC for 30 min inside a glove box. Upon cooling, these substrates were immersed in iso-propanol solution containing 8 mg/mL of CH_3NH_3I for 20 min and were then rinsed with iso-propanol. They were dried by spincoating at 4000 rpm for 30 s

and by heating at 100 ^oC for 30 min. The HTM formulation comprised of 100 mg of spiro-OMeTAD, 28.8 μL of 4-tert-butylpyridine, 17.5 μL of a stock solution of lithium bis(trifluoromethylsulphonyl) imide (520 mg/mL in acetonitrile (ACN)) and FK102 dopant (12 mg in 40 μL of ACN) in 1 mL of cholorobenzene. This HTM was spincoated at 4000 rpm for 30 s. All these process steps were carried out inside a dry box with humidity less than 15 %. A back contact of gold which is about 90-100 nm was deposited by thermal evaporation. The active area of the cell was measured to be 0.2 cm^2 which was masked by a black tape during the testing of the cells.

Device characterization: Sample purity was established using powder X-ray diffraction (PXRD). Data were collected using a Bruker D8 Advance diffractometer fitted with a CuK$_\alpha$ source operated at 40 kV and 40 mA, a 1° divergence slit, 0.3mm receiving slit, a secondary graphite monochromator and a Lynxeye silicon strip detector. A thin-film of the perovskite was deposited on FTO/TiO_2 substrate and heated at 70-100 °C for 60 min before data collection. Data were accumulated from 10 – 55° 2θ using a step size of 0.02° with a dwell time of 0.2 s per step. Pawley fits of the diffraction data were performed using TOPAS V4.1 using a pseudo-Voigt peak shape function in combination with the reported cell data for $CH_3NH_3PbI_3$ the 2H polymorph of PbI_2, $PbCl_2$ and PbICl. X-ray photoelectron spectroscopy (XPS) measurements were done using monochromatic X-ray source from Al K_α (hv=1486.7eV) and a hemispherical analyzer (EA125, Omicron). X-ray absorption spectroscopy (XAS) measurements were done in XAFCA beamline, Singapore synchrotron light source (SSLS). Top-view and cross-sectional images were recorded by Field Emission Scanning Electron Microscope (FESEM, JEOL, JSM-7600F, 5 kV). Photocurrent–voltage characteristics were recorded by applying an external potential bias to the cell while recording the generated photocurrent with a digital dual source meter (Keithley Model 2612A). The I-V measurements of the devices were done by using San-EI Electric, XEC-301S solar simulator under AM 1.5 G. Incident photon to current conversion efficiency (IPCE) was determined using PVE300 (Bentham), with a dual xenon/quartz halogen light source, measured in DC mode and no bias light is used. Incident light intensity was calibrated using a photodiode detector (silicon calibrated detector, Newport). Absorption spectra were recorded by UV-Vis-Nir Spectrophotometer (UV3600, Shimadzu) with 282 nm wavelength light source. 4-probe resistivity measurements of metal halide perovskite films were estimated using a MMR technologies variable temperature hall measurement system. The perovskite films were spun coat on soda lime glass substrates (1 cm x 1 cm) in nitrogen glove box and the resistivity measurements were performed at room temperature (302 K). 4 square electrodes (1.6 mm x 1.6 mm) of gold were thermally evaporated in square geometry onto the perovskite films. AFM images were obtained using a Asylum Research MFP3D system in tapping mode. Impedance spectroscopy was measured with an Autolab PGSTAT302N. A 20 mV voltage perturbation was applied at frequencies between 1 MHz and 0.1 Hz with the sample being illuminated by a white LED. The results were fitted using the software Z-View.

Acknowledgements

Notes and references

^aSchool of Materials Science and Engineering, Nanyang Technological University, Nanyang Avenue, Singapore 639798.
^bEnergy Research Institute @ NTU (ERI@N), Research Techno Plaza, X-Frontier Block, Level 5, 50 Nanyang Drive, Singapore 637553. E-mail:
^cSchool of Physical & Mathematical Sciences, Nanyang Technological University, SPMS-04-01, 21 Nanyang Link, Singapore 637371.
^d Engineering Sciences, A*STAR, Singapore 627833
^eSingapore-Berkeley Research Initiative for Sustainable Energy, 1 Create Way, Singapore 138602, Singapore.

Subodh@ntu.edu.sg; PBPablo@ntu.edu.sg.
†

Electronic Supplementary Information (ESI) available: AFM data illustrating the effect of Cl addition to $CH_3NH_3PbI_3$ on surface roughness of the films, cross-section FESEM image and EDX data of 50 mol % of PbCl2 addition. XRD patterns of the samples after spin-coating PbI_2 or (PbI_2+PbCl_2) and of $CH_3NH_3PbI_{3-x}Cl_x$ (x = 0.05) for different annealing conditions. J-V characteristics of 20 mol % of $PbCl_2$ cell. See DOI: 10.1039/b000000x/

References

1.   http://www.nrel.gov/ncpv/images/efficiency_chart.jpg.
2.   M. Liu, M. B. Johnston and H. J. Snaith, *Nature*, 2013, **501**, 395-398.
3.   S. D. Stranks, G. E. Eperon, G. Grancini, C. Menelaou, M. J. P. Alcocer, T. Leijtens, L. M. Herz, A. Petrozza and H. J. Snaith, *Science*, 2013, **342**, 341-344.
4.   G. Xing, N. Mathews, S. Sun, S. S. Lim, Y. M. Lam, M. Grätzel, S. Mhaisalkar and T. C. Sum, *Science*, 2013, **342**, 344-347.
5.   J. Burschka, N. Pellet, S.-J. Moon, R. Humphry-Baker, P. Gao, M. K. Nazeeruddin and M. Gratzel, *Nature*, 2013, **499**, 316-319.
6.   J. T. W. Wang, J. M. Ball, E. M. Barea, A. Abate, J. A. Alexander-Webber, J. Huang, M. Saliba, I. Mora-Sero, J. Bisquert, H. J. Snaith and R. J. Nicholas, *Nano Letters*, 2014, **14**, 724-730.
7.   H. S. Kim, C. R. Lee, J. H. Im, K. B. Lee, T. Moehl, A. Marchioro, S. J. Moon, R. Humphry-Baker, J. H. Yum, J. E. Moser, M. Graetzel and N. G. Park, *Sci. Rep.*, 2012, **2**.
8.   T. Leijtens, B. Lauber, G. E. Eperon, S. D. Stranks and H. J. Snaith, *The Journal of Physical Chemistry Letters*, 2014, **5**, 1096-1102.
9.   K. Fu, S. S. Lim, Y. Fang, P. P. Boix, N. Mathews, T. C. Sum, L. H. Wong and S. Mhaisalkar, *Nano*, 2014, 1440003.
10. S. Colella, E. Mosconi, P. Fedeli, A. Listorti, F. Gazza, F. Orlandi, P. Ferro, T. Besagni, A. Rizzo, G. Calestani, G. Gigli, F. De Angelis and R. Mosca, *Chemistry of Materials*, 2013, **25**, 4613-4618.
11. E. Edri, S. Kirmayer, A. Henning, S. Mukhopadhyay, K. Gartsman, Y. Rosenwaks, G. Hodes and D. Cahen, *Nano Letters*, 2014, **14**, 1000-1004.
12. Y. Ma, L. Zheng, Y.-H. Chung, S. Chu, L. Xiao, Z. Chen, S. Wang, B. Qu, Q. Gong, Z. Wu and X. Hou, *Chemical Communications*, 2014.
13. B. Suarez, V. Gonzalez-Pedro, T. S. Ripolles, R. S. Sanchez, L. Otero and I. Mora-Sero, *The Journal of Physical Chemistry Letters*, 2014, **5**, 1628-1635.
14. T. Baikie, Y. Fang, J. M. Kadro, M. Schreyer, F. Wei, S. G. Mhaisalkar, M. Graetzel and T. J. White, *Journal of Materials Chemistry A*, 2013, **1**, 5628-5641.
15. S. A. Kulkarni, T. Baikie, P. P. Boix, N. Yantara, N. Mathews and S. G. Mhaisalkar, *Journal of Materials Chemistry A*, 2014.
16. P. Docampo, F. Hanusch, S. D. Stranks, M. Döblinger, J. M. Feckl, M. Ehrensperger, N. K. Minar, M. B. Johnston, H. J. Snaith and T. Bein, *Advanced Energy Materials*, 2014.
17. V. Gonzalez-Pedro, E. J. Juarez-Perez, W.-S. Arsyad, E. M. Barea, F. Fabregat-Santiago, I. Mora-Sero and J. Bisquert, *Nano Letters*, 2014, **14**, 888-893.
18. A. Krishna, D. Sabba, H. Li, J. Yin, P. P. Boix, C. Soci, S. G. Mhaisalkar and A. C. Grimsdale, *Chemical Science*, 2014, **5**, 2702-2709.
19. A. Dualeh, T. Moehl, N. Tétreault, J. Teuscher, P. Gao, M. K. Nazeeruddin and M. Grätzel, *ACS Nano*, 2013, **8**, 362-373.
20. T. Krishnamoorthy, F. Kunwu, P. P. Boix, H. Li, T. M. Koh, W. L. Leong, S. Powar, A. Grimsdale, M. Gratzel, N. Mathews and S. G. Mhaisalkar, *Journal of Materials Chemistry A*, 2014, **2**, 6305-6309.
21. E. Edri, S. Kirmayer, M. Kulbak, G. Hodes and D. Cahen, *The Journal of Physical Chemistry Letters*, 2014, **5**, 429-433.
22. F. Fabregat-Santiago, G. Garcia-Belmonte, I. Mora-Sero and J. Bisquert, *Physical Chemistry Chemical Physics*, 2011, **13**, 9083-9118.
23. E. J. Juarez Perez, R. S. Sanchez, L. Badia, G. Garcia Belmonte, Y. S. Kang, I. Mora Sero and J. Bisquert, *The Journal of Physical Chemistry Letters*, 2014, **5**, 2390-2394.
24. R. S. Sanchez, V. Gonzalez-Pedro, J.-W. Lee, N.-G. Park, Y. S. Kang, I. Mora-Sero and J. Bisquert, *The Journal of Physical Chemistry Letters*, 2014, **5**, 2357-2363.
25. H. J. Snaith, A. Abate, J. M. Ball, G. E. Eperon, T. Leijtens, N. K. Noel, S. D. Stranks, J. T.-W. Wang, K. Wojciechowski and W. Zhang, *The Journal of Physical Chemistry Letters*, 2014, **5**, 1511-1515.
26. A. Yella, L.-P. Heiniger, P. Gao, M. K. Nazeeruddin and M. Grätzel, *Nano Letters*, 2014, **14**, 2591-2596.